



**POLITECNICO DI TORINO**

**DIMEAS - Department of Mechanical and Aerospace Engineering**

*College of Mechanical, Aerospace, Automotive and Production*

*Engineering*

“Master of Science in Mechanical Engineering”

**PROCESS MODELING  
OF  
THERMOPLASTIC COMPOSITES  
FOR WIND TURBINE BLADE**

PoliTo Supervisor: Dr. Maria Pia Cavatorta (Politecnico di Torino)

UML Supervisor: Dr. Marianna Maiaru (University of Massachusetts Lowell)

Student: Muhammad Fahad Mohsin

**APRIL 2021**

Thesis submitted in compliance with the requirements for the Master of Science degree

# PREFACE

This written master's thesis is based on computational mechanics' study performed remotely at University Massachusetts Lowell for thermoplastic composites. This master thesis is weighted with 18 credits in the ECT system and has completed under the "Tesi su Proposta" Program from Politecnico Di Torino, Italy. Under this program, Dr. Maria Pia Cavatorta from Politecnico Di Torino has supervised as the internal supervisor while Dr. Marianna Maiaru from University of Massachusetts Lowell has supervised as an external supervisor.

It has been an honor to work under remarkable professors and scientists in their fields and have written this thesis in their supervision. Besides the principal supervisors, I am also very thankful to my colleagues of **iComp<sup>2</sup>** group at University of Massachusetts Lowell specially Sagar Shah (Ph.D. Student) and Michael Olaya (Ph.D. student) for helping and supporting me throughout my subroutine analysis of thermoplastic composites on Abaqus software. Their feedback, support, and knowledge have been very beneficial. I am grateful to Dr. Greg Odegard and his team, in particular Swapnil Bamane (Ph.D. student) at Michigan Technological University for their collaboration related to my thesis work.

I want to express my most profound appreciation to both of my Internal and External Supervisors, for the time they dedicated to my work, for excellent assistance, for ideas on how to solve problems on the way, as well for their enthusiastic encouragement.

Finally, I would like to thank my family and friends, especially from Politecnico Di Torino, to provide extra confidence in me during this tenure.

# ABSTRACT

This work proposes process modeling simulation for future manufacturing of wind turbine blades using fully recyclable thermoplastic composites. The formation of crosslinks in thermosets composites makes them non-eco-friendly and difficult to recycle, resulting in a massive amount of composite material to the waste stream. The use of thermoplastic resins versus their thermosetting counterparts can potentially introduce cost savings due to non-heated tooling, shorter manufacturing cycle times, and recovery of raw materials from the retired part.

Thermoplastic resin systems have long been discussed for use in large-scale composite parts but have yet to be exploited by the wind energy industry because of their manufacturability. A newly developed ELIUM thermoplastics by Arkema has been studied for its unique combination of mechanical properties and manufacturability. ELIUM is characterized by high impact resistance, post-thermoform ability, and it is fully recyclable. Additionally, ELIUM can be manufactured through infusion and in-situ polymerization, enabling mass production of large components. Specifically, ELIUM-150 is used in this work, which has a low viscosity and will be suitable for manufacturing wind blades through the infusion process. Process modeling is performed using Abaqus to predict the temperature evolution and Degree of Polymerization via user-written subroutines. A wind turbine blade geometry is modeled accounting for its various components, composite lay-ups, and manufacturing cycle. Additional modeling is proposed to analyze the spar-cap area of the blade. An optimization study is performed to determine a polymerization cycle that would guarantee the fastest possible time to homogenously polymerize the composite wind blade while maintaining a low exothermic heat of reaction during manufacturing.

# Contents

1	Introduction .....	6
1.1	Background .....	9
1.2	Motivation.....	10
1.3	Aims and Objectives.....	11
1.4	Novelty .....	12
1.5	Chapters Distribution .....	12
2	Thermoplastics Literature Review .....	14
2.1	Classification of Thermoplastics: .....	14
2.1.1	Vinyl polymerization .....	15
2.1.2	Ring-opening polymerization.....	15
2.2	Elium Thermoplastics:.....	16
2.2.1	Typical Curing Characteristics .....	16
2.2.2	Curing Time .....	17
2.2.3	Effects of Flow Mesh Length .....	18
2.2.4	Effects of Multi Vacuum Levels.....	18
2.2.5	Effects of Phase change materials .....	20
2.2.6	Rheology and shrinkage data for simulation .....	20
2.2.7	Cone Calorimeter Test .....	21
2.2.8	Differential Scanning Calorimetry (DSC) .....	22
2.2.9	Degree Of Conversion (DOC) .....	22
2.2.10	Thermo Gravimetric Analysis (TGA).....	23
3	Manufacturing of Wind Blade.....	24
3.1	Thermosets .....	24
3.2	Thermoplastics.....	24
4	Process Modelling of Wind Blades.....	26
4.1	Introduction .....	26
4.2	Application of Classical Laminate Theory .....	28
4.2.1	Hooke's law utilization in CLT .....	28
4.2.2	Assumptions for Classical Laminate Theory.....	29
4.2.3	Hooke's Law for Lamina under plane stress state .....	30

4.2.4	Stress Distribution in Symmetric and Non-Symmetric Laminate.....	31
4.2.5	Resultant forces and moments due to thermal load.....	33
4.2.6	Overall CTE for the laminate and total strain due to thermal load .....	33
4.2.7	Residual stresses in the laminate due to thermal load.....	34
4.2.8	Thermal strain and change in height through the thickness .....	34
4.2.9	Validation of results through Abaqus Simulation .....	35
4.2.10	Validation of results through CLT Software .....	35
4.3	Process Modelling with Thermoplastics .....	36
5	Results and discussion .....	37
6	Conclusion and recommendations .....	39
6.1	Future Directions: .....	39
	Nomenclature .....	40
	References .....	42
7	List of tables .....	46
8	List of figures.....	46

# Chapter#1

## 1 Introduction

Fiber reinforced thermoplastic composites (FRTPCs) are widely used in high-end aerospace and aircraft industries due to their high strength-to-weight ratio, fracture toughness and damage tolerance. The processing speed of thermoplastic composites is relatively fast as compared with their thermoset counterparts. In general, a melt process is used to manufacture structural FRTPCs in which the thermoplastic resin is melted, formed and solidified. The significant drawbacks of this thermal processing are the high processing temperatures and pressures together with relatively high viscosity of the thermoplastic material which limit the manufacturing of FRTPC parts in size and thickness [1]. An alternative to melt processing of the FRTPCs is the in-situ polymerization of monomeric or oligomeric thermoplastic materials. Some examples of reactive thermoplastic resins are the thermoplastic polyurethanes (TPUs), polyamides (PAs), polyethyleneterephthalate (PET), polybutyleneterephthalate (PBT) and Polycarbonate (PC) [1]. Another example is the recently developed Elium® acrylic resin which is composed of 2-Propenoic acid, 2-methyl-, methyl ester or methyl-methacrylate monomer (MMA) and acrylic copolymers in which MMA undergoes a free radical polymerization to its polymer PMMA. The advantage of commercially available Elium® is that the polymerization can take place at relatively low temperatures even at room temperature. In reactive processing of Elium® composites, the fiber reinforcements are first impregnated with the resin which is in a liquid state at room temperature with a relatively low viscosity. Afterwards, the in-situ polymerization takes place by mixing the MMA monomers with compatible initiator systems such as a peroxide and applying stimuli such as heat, microwave or ultraviolet. One of the major challenges in processing fiber reinforced Elium® composites is the presence of internal overheating due to the exothermic reaction of the radical polymerization which is also seen in thermoset resins during the curing or cross-linking of the molecular groups. This might result in boiling of the thermoplastic resin and hence voids in the composite part. In addition, the large temperature difference can take place in thick composite manufacturing, which results in unwanted residual stresses and shape distortions

as extensively investigated in thermoset composites [2–4]. Therefore, the polymerization reaction of Elium® composites has to be understood, described and predicted well in order to develop reliable FRTPCs by using the reactive manufacturing processes such as vacuum assisted resin transfer molding and pultrusion. The previous researches on Elium® resins and their composites are summarized in the following. Barbosa et al. [5] compared the behavior of Elium® 150 in mode II interlaminar fracture with the traditional epoxy matrix, and found that it can resist up to 40% more than epoxy matrix composites based on the end notched flexure tests. With the optimized welding parameters of a weld time of 1.5 s and a weld pressure of 3 bar, the maximum lap shear strength of the welded carbon/Elium® composite laminate was found to be 23.2% higher than the adhesively bonded Elium® laminates [6]. Bhudolia et al. [7] studied mode I interlaminar fracture toughness (ILFT) behavior of Elium® composites. The results showed that the ILFT properties of thin ply thermoplastic composites was found to be 30% higher than the thick ply thermoplastic composites. Zoller et al. [8] optimized the process temperature by analyzing the radical polymerization of the acrylic resin and compared the conversion degree of the resin with different types of initiators. Elium® composites exhibited lower damage and higher residual strain than the epoxy composite through the load-unload cycles as reported in [9]. The advantage of the Elium® resin composite system in the vibration damping was presented in [10] by vibration and dynamic mechanical analysis tests and its structural damping was found to be 27% higher than the epoxy composites. Boumbimba et al. [11] found that the addition of acrylic tri-block copolymers led to an increase in impact resistance for test temperatures of 80 °C. This improvement was approximately 24% in terms of the penetration threshold. Kinvi-Dossou et al. [12] investigated the impact performances of Elium® composites and found that the delamination extension of acrylic composite was smaller than the one for epoxy composites. In addition, the moisture diffusion behavior of Elium® composites was investigated in [13]. The results indicated that the weight gain at the saturation of flax-acrylic composite was found to be lower than that of flax-epoxy composite. The characterization of Elium® 150 polymerization reaction was studied in [14] and it was shown that the polymerization was influenced both by the peroxide initiator and the temperature. An optimized thermal cycle for the polymerization of Elium®150 resin was proposed in Cadieu et al. [15] studied the loading rate effect on the mechanical properties of a glass/Elium® 150 laminated composites. The

results indicated that the loading rate had a significant influence on the macroscopic parameters of the behavior of the samples. Nash et al. [16] investigated the effect of environmental conditioning on the apparent interlaminar shear strength and dynamic mechanical properties of well-established marine resin systems- and Elium® -matrix composite materials. It was demonstrated that the infusible Elium® resin could be a candidate for the use in marine structures. Kazemi et al. [17] studied the mechanical properties of an ultra-high-molecular-weight polyethylene fabric/Elium® laminates and found that Elium® can be a competitive resin to replace the traditional resins for the fabrication of composite structures. An advanced cure monitoring system and a microwave system were developed and utilized to manufacture Elium® composites in [18]. The temperature evolution and resistance of Elium® composite were determined to obtain a better microwave heating by achieving a 25% increase in the speed of Elium® reaction. The chemical kinetics and rheology of a partially polymerized carbon/PMMA prepregs were investigated in [19] to develop materials processing guidelines for reactive thermoplastic prepregs.

Although Elium® thermoplastic resins and their composites were investigated by several researchers, to date there has been a limited focus on the exothermic reaction and resulting polymerization over- heating in literature. It was stated in [20] that the highly exothermic reaction during the manufacturing of thick Elium® composites (12 mm or greater) could cause the peak temperature being higher than the resin boiling temperature of 100 °C. This might cause an uncontrolled temperature distribution and growth as well as process instabilities and unwanted monomer loss due to the boiling of the resin. The objective of this paper is therefore to critically assess the exothermic reaction and overheating during manufacturing Elium® composites which have been overlooked in the literature. The polymerization kinetics of the Elium® resin is investigated by performing isothermal and dynamic differential scanning calorimetry (DSC) tests. To this end, a temperature dependent kinetics model is developed based on the data fitting analysis. The obtained kinetics model and the total heat of polymerization reaction are used in the transient thermo- chemical model to predict the temperature and degree of polymerization (DoP) evolutions during the manufacturing process. First, the transient thermo-chemical model is validated by measuring the temperature evolution during the reactive processing of the pure Elium® resin at different temperatures in a water bath. Then, the validated polymerization process model is used to



predict the temperature evolution and overheating during the vacuum infusion process of glass fiber reinforced Elixir® laminates with different thicknesses and process temperatures. The model predictions are compared with the measurements. The quality of the produced laminates with different thickness are evaluated by performing a microscopy analysis for the cross sections of the manufactured laminates.

## 1.1 Background

Fiber-reinforced polymer composites are a desirable class of structural engineering materials due to their high specific mechanical properties. They are increasingly used in the construction, automotive, aerospace, and energy sectors (Mazumdar et al., 2017). Electricity generated from wind turbines has grown consistently by approximately 7.3 GW of installed capacity every year for the last decade in the United States (American Wind Energy Association, 2017). Wind turbine blades are constructed with fiber reinforced polymer and balsa or foam core; landfilling turbine blades contributes a massive amount of composite material to the waste stream. One study estimates 9.6 metric tons of composite per megawatt of installed capacity (Arias, 2016). Such waste of highly engineered material represents not only an environmental issue, but also a loss of potentially recoverable capital. Thermoplastic resins, which are inherently recyclable (Jacob, 2011), are potentially a better design choice due to increasing regulation of composite waste landfilling. The European Union Directive on Landfill Waste has enacted legislation that prohibits disposal of large composite parts such as wind turbine blades (1999/31/EC). It is prudent to anticipate the potential for similar legislation in the United States; therefore, it is a primary objective of the Institute of Advanced Composites Manufacturing Innovation to qualify composite technologies of which 80% of the constituent materials can be reused or recycled (IACMI, 2018).

Thermosetting resins such as epoxy, vinyl ester, and poly(urethane) dominate the composites market; the wind industry exclusively uses these resins for vacuum infusion of blades. However, there is an increasing trend toward using thermoplastic resins in long fiber composites outside of the wind industry and a growing interest for using these resins for blade fabrication (Yao et al., 2018). Presently, there are several options for wind turbine blades at the end of their service lives: direct deposit in a landfill, grind for use as aggregate in concrete, or incineration with energy recovery (Correia et al., 2011; Fox, 2016; Larsen,

2009; Papadakis et al., 2010; Ribeiro et al., 2015). Additionally, a recent study has shown that thermoset blades can be recycled via grinding to be used for construction materials (Mamanpush et al., 2018). That these recycling techniques are not commercially exploited on a large scale demonstrates the small margins on which they operate. Thermoplastics can potentially limit the extent of down-cycling that thermoset composites require. Still, the viability of composite recycling is heavily dependent upon reintroduction of recovered materials into the supply chain to displace virgin materials (Li et al., 2016; Witik et al., 2013).

The current investigation quantifies and demonstrates the methods by which the Elium thermoplastic resin system (Arkema, 2018) can facilitate recycling of large-scale composite parts by recovering and reusing material from a component of a wind turbine blade. A portion of a spar cap, which acts as the end of the I-beam structure in the interior of the blade, was used for this study. Four recycling techniques are considered, including thermal decomposition of the polymer matrix, mechanical grinding, thermoforming, and dissolution. The decomposition energy of a commercial epoxy and Elium are compared via simultaneous thermal analysis (STA), which combines thermogravimetric analysis (TGA) and differential scanning calorimetry (DSC). The tensile properties of recycled thermoplastic regrind are compared to those of similar virgin material. Thermoforming is demonstrated on a thermoplastic spar cap, and test panels are thermoformed to make a prototypical skateboard. Energy requirements for dissolution of thermoplastic components and separation into their constituent materials are estimated. Further, the tensile mechanical properties of glass fibers recovered from the dissolution experiment are compared to those of virgin glass fibers. Dissolution of thermosets is not possible, and therefore only the thermoplastic system is investigated using this recycling technique. Finally, the technical results from the investigation of the dissolution technique are used in an economic analysis to assess the commercial viability of recycling.

## 1.2 Motivation

Wind turbine blades are complex structures whose design involves the two basic aspects of

- Selection of the aerodynamic shape

- Structural configuration and materials selection (to ensure that the defined shape is maintained for the expected life)

Modern blades

- consist of different kinds of materials (typically composite materials in monolithic or sandwich configuration)
- use various connections solutions between different substructures - include many material or geometric transitions

The growth rate of blade mass with length has been reducing in the past decades Key drivers for reduction:

- Improved manufacturing processes
- Introduction of new materials
- More efficient use of materials and improved structural configurations

## 1.3 Aims and Objectives

This study's objective was to work on an alternative material for the manufacturing wind turbine blade. Thermoplastic resin systems have long been discussed for use in large-scale composite parts but have yet to be exploited by the energy industry. The use of these resins versus their thermosetting counterparts can potentially introduce cost savings due to non-heated tooling, shorter manufacturing cycle times, and recovery of raw materials from the retired part. Because composite parts have high embedded energy, recovery of their constituent materials can provide substantial economic benefit. This study determines the feasibility of recycling composite wind turbine blade components that are fabricated with glass fiber reinforced Elixir® thermoplastic resin. Several experiments are conducted to tabulate important material properties that are relevant to recycling, including thermal degradation, grinding, and dissolution of the polymer matrix to recover the constituent materials. Dissolution, which is a process unique to thermoplastic matrices, allows recovery of both the polymer matrix and full-length glass fibers, which maintain their stiffness (190 N/(mm g)) and strength (160 N/g) through the recovery process. Injection molded regrind material is stiffer (12 GPa compared to 10 GPa) and stronger (150 MPa

compared to 84 MPa) than virgin material that had shorter fibers. An economic analysis of the technical data shows that recycling thermoplastic glass fiber composites via dissolution into their constituent parts is commercially feasible under certain conditions. This analysis concludes that 50% of the glass fiber must be recovered and resold for a price of \$0.28/kg. Additionally, 90% of the resin must be recovered and resold at a price of \$2.50/kg.

## **1.4 Novelty**

In this thesis, numerical simulations have performed to develop a model for wind turbine blade that can be manufacture through thermoplastic material. For thermoplastic material, it is described about recently developed chemical compound named as Elium by Arkema company. Elium® resins can be moulded by infusion at room temperature to make large and stiff structural parts, with excellent toughness. Low viscosity and long gel time ensure excellent fiber impregnation to reach optimum mechanical properties. Carbon fiber and glass fiber can be used. Structural bonding is possible with AEC Polymers adhesives.

## **1.5 Chapters Distribution**

This thesis is divided into six main sections (Chapters).

Chapter 1 (Introduction) is about relevant background theory, which provides an overview of this study, aims and objectives, and novel approaches for the process modelling of thermoplastic composites.

Chapter 2 (Literature review) contains the theory related to the thermoplastics, its classification, different types of equipment and material used for its application, and the effects of different parameters on polymerization process.

Chapter 3 (Manufacturing of Wind Blade) describes the manufacturing processes and details related to the components being used to build up the complete structure of blade.

Chapter 4 (Process Modelling of Wind Blades) explains the polymerization kinetic model along with description of all boundary conditions applied in sub routine analysis.

Chapter 5 (Results and discussions) In this section, the results from the study have discussed the graphs and images obtained from Abaqus Software.

Chapter 6 (Conclusion and recommendations) concludes the aim of the experimental study and the overall summary of the research along with the future directions to extend the process modelling of thermoplastics composites for wind turbine blade.

# Chapter #2

## 2 Thermoplastics Literature Review

Thermoplastic polymers differ from their thermoset counterpart primarily by their melt temperature being lower than their decomposition temperature, while thermoset polymers have melting temperatures higher than their decomposition temperature, meaning that they cannot be reshaped upon melting. In molecular terms, this characteristic can be correlated to molecular weight, since an increase in molecular weight increases the melting temperature. Thermoset have very high molecular weights because of the cross-links between their polymer chains, while thermoplastics have lower molecular weight since they are generally not cross-linked.

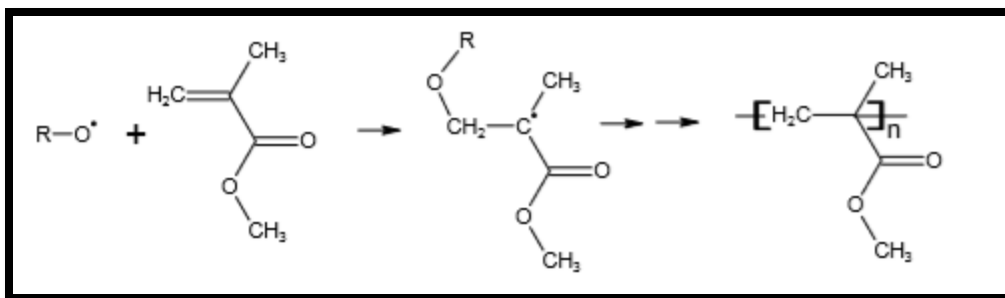
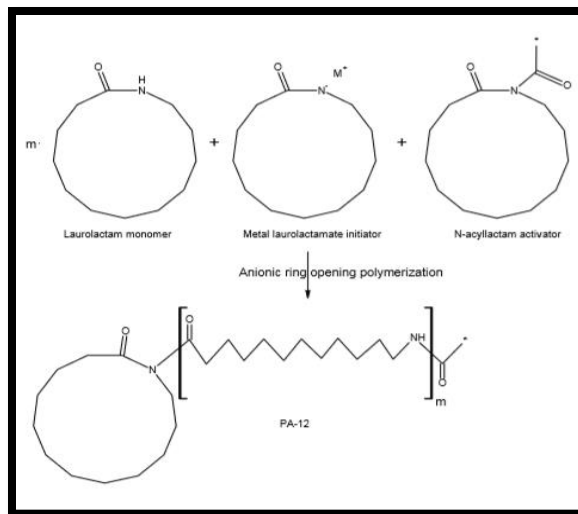
The fundamental difference in physical properties between thermosets and thermoplastics has governed the development of their respective manufacturing techniques over the years with thermoplastic usually being melt processed while thermosets are exclusively reactively processed.

### 2.1 Classification of Thermoplastics:

Most thermoplastics have a high molecular weight. The polymer chains associate by intermolecular forces, which weaken rapidly with increased temperature, yielding a viscous liquid. In this state, thermoplastics may be reshaped and are typically used to produce parts by various polymer processing techniques such as injection molding, compression molding, calendaring, and extrusion. [3][4] Thermoplastics differ from thermosetting polymers (or "thermosets"), which form irreversible chemical bonds during the curing process. Thermosets do not melt when heated, but typically decompose and do not reform upon cooling. Based on the polymerization reaction, thermoplastics has been divided in 2 following types;

### 2.1.1 Vinyl polymerization

Vinyl polymers are polymers made from vinyl monomers: small molecules containing carbon carbon double bonds. During polymerization the double bonds are broken into single bonds, resulting in two free electrons. Then these monomer units will form a long chain of many thousands of carbon atoms containing only single bonds between atoms. Examples are Polyethylene, Polypropylene, Polystyrene, Poly methyl metacrylate (Elum) etc.



### 2.1.2 Ring-opening polymerization

Ring-opening polymerization (ROP) is based on a polymerization mechanism in which ring-shaped molecules (cycles) are opened into linear monomers or oligomers and subsequently connected into high molecular weight polymers without generating byproducts. The role of the initiator is to provide the polymeric chain with the necessary electrical charge for chain - growth in its anionic form ( $C_6H_{10}ON$ ). The activator consists of derivated species from caprolactam, in which a carbamoyl group has been attached to its nitrogen atom. Examples are Polyethers, Polyamides etc.

## 2.2 Elium Thermoplastics:

FRPC laminates with traditional thermoplastic resins, namely PEEK, Cyclic Butylene Terephthalate (CBT), Polyurethanes (PU), to name but a few, are already well documented in the literature [3–6]. These resins are in film or pellet forms, which require high processing temperature and costly equipment [7]. As a result, compared to thermoset resins, they are rarely used [8–10]. Essentially, a room temperature curing thermoplastic resin is needed, which not only does not compromise the mechanical properties of composites, but also can be processed using liquid processing techniques like Vacuum Assisted Resin Infusion (VARI) and Resin Transfer Molding (RTM). The ELIUM® 150 is a low viscosity liquid, thermoplastic resin for infusion and RTM processes. Through the use of the same low pressure processes and equipment used today to produce thermoset composite parts, these formulations lead to the production of thermoplastic composites reinforced by continuous glass, carbon or natural fibers. The resulting thermoplastic composite parts show mechanical properties similar to those of parts made of epoxy resins while presenting the major advantages of being postthermoform able and recyclable and of offering new possibilities for composite/composite or composite/metal assemblies. The Elium® resin is a very promising resin for the production of recyclable advanced thermoplastic composites that can be used in a wide range of applications.

### 2.2.1 Typical Curing Characteristics

The ELIUM® resins are 2K based formulations that undergo radical polymerization to produce thermoplastic composite matrices. The polymerization is initiated by Peroxide compounds (Luperox®). Typical open time and peak time with 3% Luperox® EZ-FLO are:

Reactivity <sup>(2)</sup> (200 grams)	Infusion open time	Injection open time	Peak time
15 °C	30 min.	35 min.	50 min.
20 °C	25 min.	30 min.	40 min.
25 °C	20 min.	25 min.	33 min.

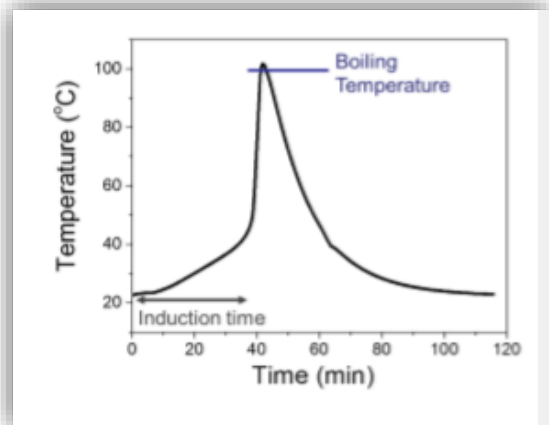
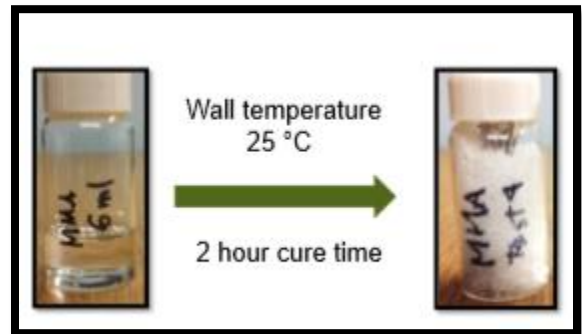
The demolding can take place 5-10 minutes after reaching the peak exotherm. Open time is the amount of time during which the viscosity of the resin is low enough to inject the



resin. Temperature and peroxide ratio will affect the open and peak times. The recommended peroxide ratio is from 1,5% (slow reactivity) to 3% (higher reactivity). Out of this range the resin will not polymerize properly. Room temperature polymerization leads to high conversion rate, so post-curing is generally not needed. If maximum mechanical properties are desired, post-curing at 80 °C for 4 hours is beneficial. Vinyl ester or epoxy molds with a glass transition of 100-120 °C are recommended.

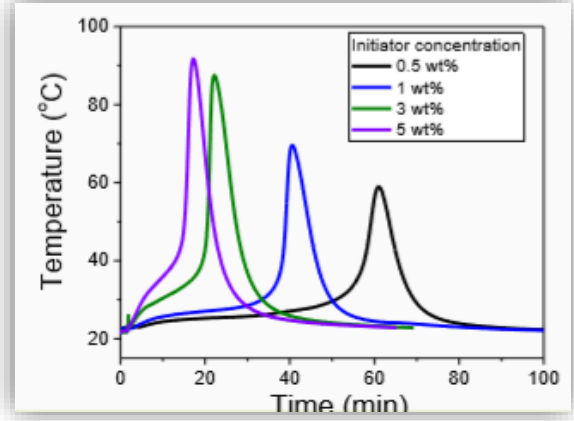
### 2.2.2 Curing Time

Samples of Methyl Methacrylate (MMA) monomer immersed in constant T bath with J-Type thermocouples. Traditional thermoplastic resins, namely PEEK, Cyclic Butylene Terephthalate (CBT), Polyurethanes (PU), to name but a few, are already well documented in the literature. These resins are in film or pellet forms, which require high processing temperature and costly equipment. As a result, [2] compared to thermoset resins, they are rarely used. Essentially, a room temperature curing thermoplastic resin is needed, which not only does not compromise the mechanical properties of composites, Initiator is analogous to hardener / curative in epoxy systems. Less initiator means slower reaction and lower peak temperatures due to increased time for heat transfer.



### 2.2.3 Effects of Flow Mesh Length

The carbon non crimp fiber (NCF) was first infused with full flow mesh (same as the size of the panel). However, the full flow mesh accelerated the flow in the longitudinal direction, the panel was not fully infused in the thickness direction, and a massive dry spot with entrapped air was noticed. Then, the infusion was carried without the flow mesh as shown in Figure to reduce the longitudinal resin flowrate. However, this attempt was not successful. The infusion was too slow and resin reached its gel time before the infusion was complete. Further, the panel was infused with reduced flow mesh length and resulted in much improved impregnation with only a small dry spot as shown in Figure. The flow mesh length (per cent of the total laminate length) was varied from 50% to 80% to achieve the right balance between the preform filling and the impregnation time. Preform was better filled with reduced flow mesh lengths as compared to one with no and full flow mesh length.



		Flow Mesh Length (Per Cent of Total Laminate Length)					
		0%	50%	60%	70%	80%	100%
Observations on preform filling at 400 mbar infusion	Top surface of laminate	Cannot fully infuse (Figure 7a)	Small dry spot	Smaller dry spot	Small dry spot	No dry spot (Figure 7b)	No dry spot (Figure 7c)
	Bottom surface of laminate	Cannot fully infuse (Figure 7a)	Massive dry spot	Massive dry spot	Small dry spot	Very small dry spot (Figure 7b)	Massive entrapped air (Figure 7c)
Quality		Not acceptable	Not acceptable	Not acceptable	Not acceptable	Acceptable	Not acceptable

### 2.2.4 Effects of Multi Vacuum Levels

Even though the thickness infusion was found to be significantly improved by reducing the flow mesh length, it was necessary to optimize the vacuum level and corresponding flow speed which has a detrimental effect on manufacturing of NCF laminates with low void content. Infusion of NCFs with both the matrices was carried out with one-, two-, and three-stage vacuum levels. The details of the vacuum levels used in single and multi-stage phases



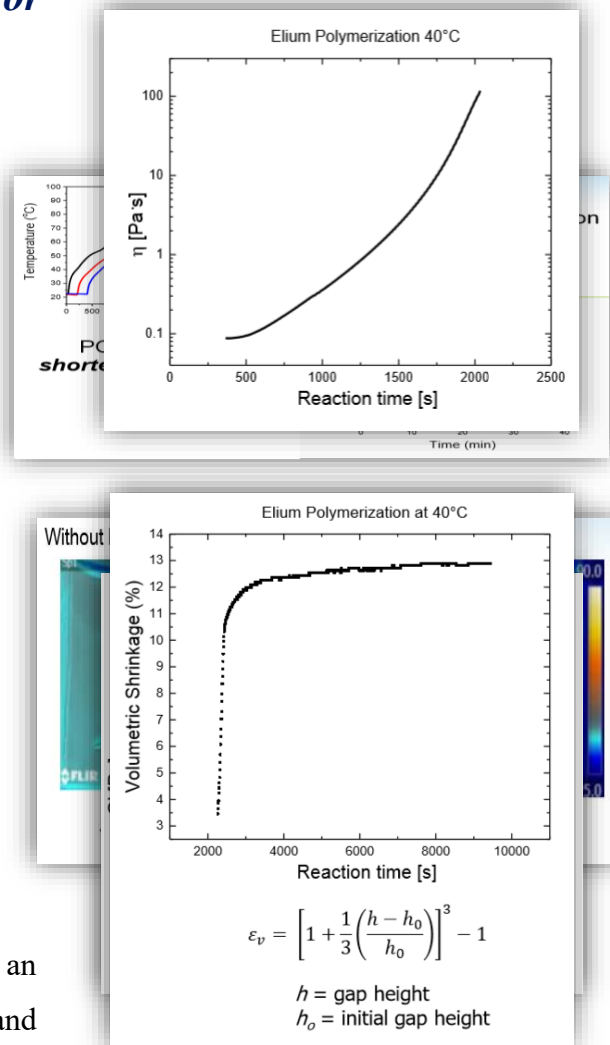
### 2.2.5 Effects of Phase change materials

Phase Change Materials (PCMs) are substances which absorb or release large amounts of so-called “latent” heat when they go through a change in their physical state, i.e., from solid to liquid. With the thermal scanning, it can be seen that without PCM there is a Slow motion during the curing reaction the resin is transferred through the bag into the laminate, distributed by a channel or lining/mesh. Single stage infusion was carried out at similar infusion and consolidation vacuum levels.

Two-stage infusion was used where first the resin was infused at low vacuum levels for balancing the impregnation in the longitudinal and transverse direction. Once the infusion was completed, the consolidation was carried out at higher vacuum level.

### 2.2.6 Rheology and shrinkage data for simulation

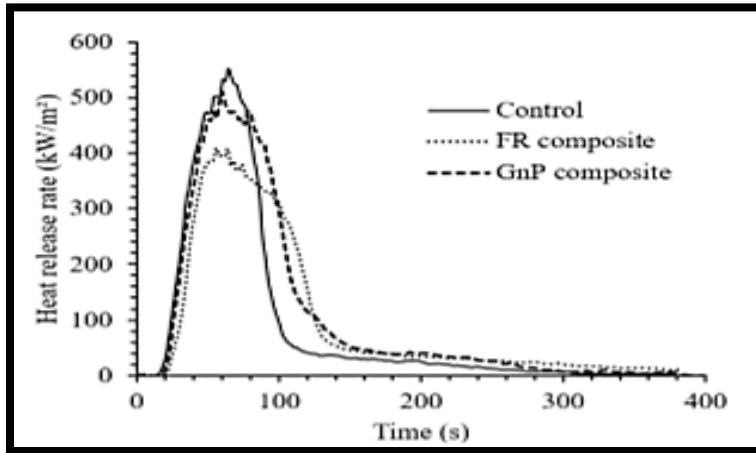
Measure the viscosity as a function of time at a constant shear rate of 100 1/s with the gap fixed at 1 mm. Such a viscosity correlation is particularly useful – because the intrinsic viscosity is a function of molecular weight, the concentration needed to obtain a given viscosity for any given average molecular weight can be calculated. This viscosity correlation also provides a link to the kinetic models that can predict conversion. Storage modulus ( $E'$ ) is a measure of elastic response of a material. It measures the stored energy. When the torque on the geometry reaches a cutoff value, switch to an oscillatory measurement at 3.33 rad/s and



allow the gap to change to produce an applied normal force of 0.5 N. The plots the trends of the normalized storage modulus ( $E_0$ ) and the loss tangent ( $\tan\delta$ ) are represented as a function of temperature. This test allows the detection of all the thermal transitions of the tested specimens in the selected temperature range. Elium has a high amount of volumetric shrinkage up to 13% with having storage modulus 1MPa.

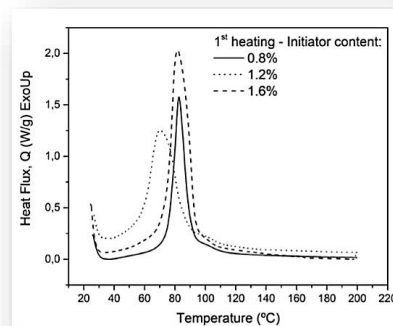
### ***2.2.7 Cone Calorimeter Test***

Heat release and smoke production behavior of the composites were analyzed on a cone calorimeter fabrics were placed between two layers of FR (flame retardant) mats. Sample dimensions of 100 mm  $\times$  100 mm were exposed to a heat flux of 35 kW/m<sup>2</sup> in accordance with ISO 5660–1 graphene nano-platelet. The FR composites were designated after their commercial mat grades, namely, E20MI, E11MIL, T6663 and T6594. The Control composite without the FR coating mats was produced for comparison of properties.



### 2.2.8 Differential Scanning Calorimetry (DSC)

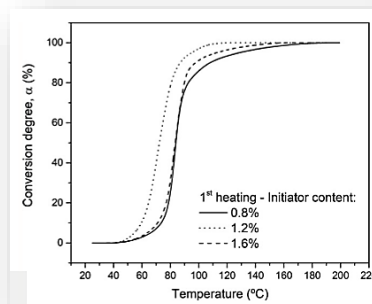
To study the influence of the peroxide initiator in the polymerization, differential scanning calorimetry (DSC) is a thermo analytical technique in which the difference in the amount of heat required to increase the temperature of a sample and reference is measured as a function of temperature. Samples with 0.8% and 1.6% initiator contents present no significant variation in the onset temperature values, and the reaction in both cases starts at approximately 75°C. Total heat of the reaction is dependent on the molecular weight of the formed chains. The theoretical heat of polymerization of MMA is  $-550$  J/g.



Initiator content in weight (%)	$T_{\text{onset}}$ (°C)	$T_{\text{max}}$ (°C)	$-\Delta H$ (J/g)
0.8	75.9	82.6	129.4
1.2	57.9	70.4	150.7
1.6	74.0	81.8	210.7

### 2.2.9 Degree Of Conversion (DOC)

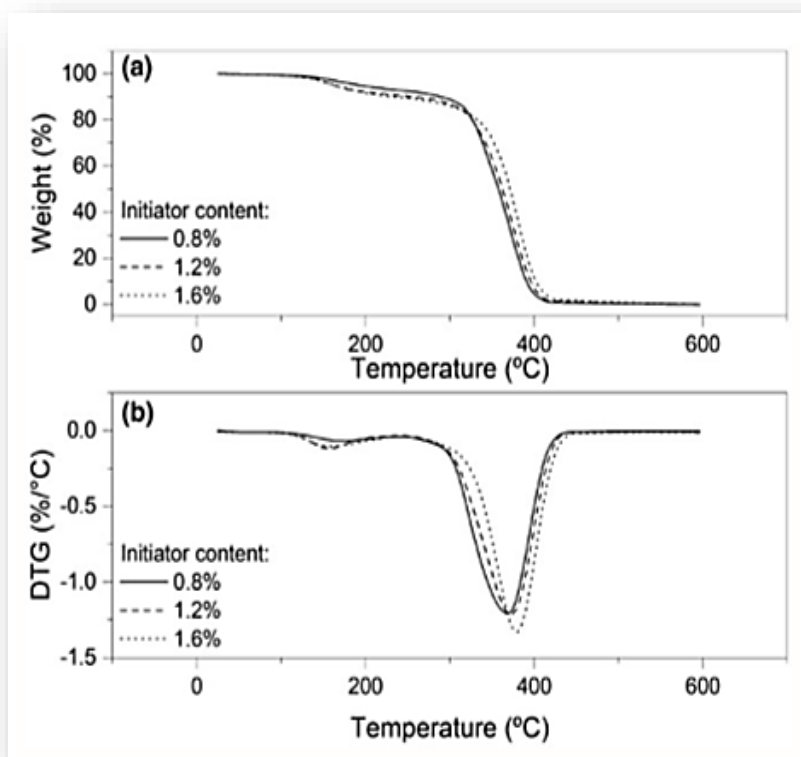
Conversion or polymerization degree ( $\alpha$ ) calculated as a function of the temperature (T). The results for each initiator concentration are presented in Figure. The three curves present two plateaus separated by an exponential growth region. Even though the DSC results do not allow the determination of the exact limit between the polymerization reaction steps, it is reasonable to assume that the first plateau is mainly associated with the induction period that precedes the initiation and propagation of the reaction. This latter propagation stage is, therefore, represented by the exponential growth region, which takes place until reaching its termination at the second plateau.



Initiator content in weight (%)	$T_{\text{gDSC}}$ (°C)
0.8	97.7
1.2	95.8
1.6	90.0

### 2.2.10 Thermo Gravimetric Analysis (TGA)

Thermo gravimetric analysis (TGA) and DTG curves are presented in Figure 8 for all three samples with 0.8%, 1.2%, and 1.6% in mass content of initiator. From these curves it can be noticed that the three samples present only minor differences in the decomposition behavior. DTG is a type of thermal analysis in which the rate of material weight changes upon heating is plotted against temperature and used to simplify reading the weight versus temperature thermogram peaks which occur close together. The thermal decomposition, regardless the initiator content, occurred in two stages and was completed in temperatures below 500°C, reaching 100% in weight loss.



# Chapter#3

## 3 Manufacturing of Wind Blade

### 3.1 Thermosets

### 3.2 Thermoplastics

Based on RTM manufacturing principles, the vacuum infusion technique uses a solid mold half and a flexible mold half (usually a plastic film) instead of a set of two solid mold halves. Due to the flexible mold half, processing pressure is limited to atmospheric pressure.

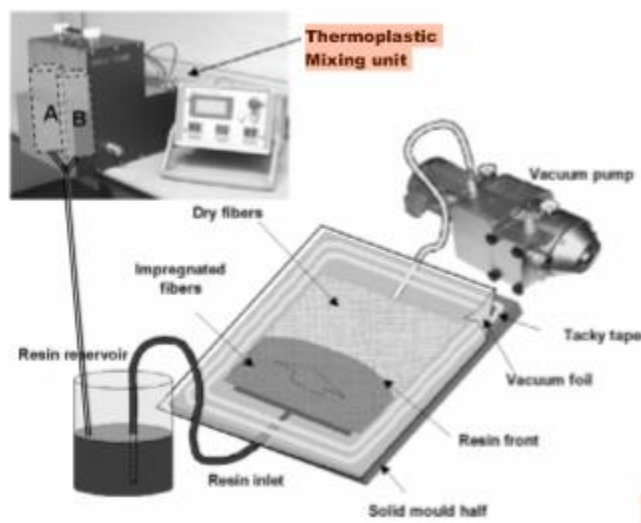


Figure 3.12: Typical resin infusion process for thermoplastic composites (adapted from [20]).

As with RTM, the first step of the process involves placing a dry fiber pre-form on the surface of the solid mold half (see Figure 3.12). The second step consists of covering the mold with a flexible medium, in this case, either a vacuum bag or a semi-rigid mold half (also known as light RTM). Once the vacuum is pulled between the flexible and the solid mold halves, the resin system can be introduced by opening an inlet valve. Resin is then forced to flow toward the outlet port connected to the vacuum pump. Once the pre-form is fully impregnated, the inlet port is closed and the part is



left to polymerize before being released from the mold. As with RTM, isothermal or non-isothermal processing is possible depending on the resin system. In all cases, the resin reservoirs must be kept above the melting temperature of the different components of the polymer reactive system and the mold must be kept at the polymerization temperature. Compared to RTM, vacuum infusion has the advantage of being low-cost and allows the manufacture of significantly larger parts. However, infusion time is longer due to low processing pressure and poor surface finish will always be obtained on the flexible mold side. Also, since vacuum bags and other consumables are generally not reusable, the process should be considered less sustainable. Vacuum infusion of thermoplastic composites has also not yet been used on an industrial scale, but different systems and manufacturing techniques were investigated over the past decade. Significant progress in process development for anionic polyamide-6/glass composites was achieved at Delft Technical University [21] and infusion of APA-6 on carbon fibers was investigated at the University of Alabama [22].

# Chapter # 4

## 4 Process Modelling of Wind Blades

The production of rotor blades for wind turbines is still a predominantly manual process. Process simulation is an adequate way of improving blade quality without a significant increase in production costs. This paper introduces a module for tolerance simulation for rotor-blade production processes. The investigation focuses on the simulation of temperature distribution for one-sided, self-heated tooling and thick laminates. Experimental data from rotor-blade production and down-scaled laboratory tests are presented. Based on influencing factors that are identified, a physical model is created and implemented as a simulation. This provides an opportunity to simulate temperature and cure-degree distribution for two-dimensional cross sections. The aim of this simulation is to support production processes. Hence, it is modelled as an in situ simulation with direct input of temperature data and real-time capability. A monolithic part of the rotor blade, the main girder, is used as an example for presenting the results.

### 4.1 Introduction

The production of rotor blades for wind turbines is still a predominantly manual process. In order to improve blade quality without a significant increase in production costs, tolerance management is combined with statistical process control. A process model with both analytical and numerical elements is developed, based on statistical production data and experiments. The investigation presented here focuses on the simulation of temperature distribution for one-sided, self-heated tooling and thick laminates. The model includes the properties of the heating system and the exothermic behavior of resin. The simulation is linked to experiments with varying process temperatures and laminate thicknesses. Even if the geometry of rotor blades is not as complex as an airplane wing cover, different zones have to be taken into account. In Figure 1, a generic cross section of a rotor blade is shown. The main, girders (yellow), and possibly minor girders, are made of unidirectional glass or carbon-fiber reinforced plastics. Non-crimped fabric, pre-impregnated fibers or rovings can be used as raw materials according to the company-specific production process. As the girders take the main

bending loads, the laminate quality of these parts is crucial. Torsional loads are carried by the shells and shear webs (turquoise). Therefore, a higher moment of inertia is required. In order to achieve this without unnecessary weight gain, sandwich material is used for shells and shear webs. Thin glass-fiber top layers cover a polyethylene terephthalate (PE/PET) foam core. Sometimes, in regions of higher loads, balsa core material is also used.

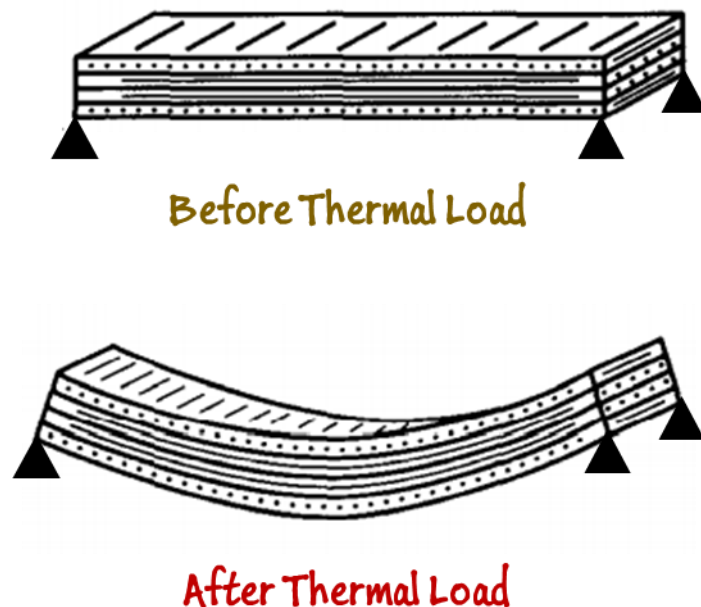
The girders are prefabricated parts and connected with the shells by the infusion process (Figure 2). Shells are joined to each other and with the shear webs in a bonding process with thixotropic adhesives for secondary bonding lines (purple). Materials 2017, 10, 1157 2 of 12

A general structure of a rotor blade middle section, including the material distribution described, is summarized in Figure 1. Figure 1. Typical cross section of a rotor blade according to [1–3]. Figure 1 only shows the outer (tip) section of a rotor blade. In the root section are zones with wall thicknesses of up to 100 mm made of triaxial glass-fiber composite for the load transfer between blade and hub. The production process of rotor blades includes the prefabrication of girders, shear webs, parts of root sections, and additional smaller parts. These are joined to the suction or pressure side shell, respectively, by a liquid resin infusion process. In most cases, the shear webs (one or more) are bonded to one shell and cured. Blind bonding is the final production step of the blade blank. Here, the shells and the shear webs are connected to a closed rotor blade. The central production step for manufacturing fiber-reinforced plastics for wind-turbine applications is the infusion process. As each manufacturer has their own special features, Figure 2 shows a general overview of a vacuum-assisted resin infusion (VARI) process. In Figure 2, a generic part of dry fabric is impregnated with epoxy resin. For rotor blades, in the majority of cases non-woven fabric is used. The infusion is driven by pressure differences between the low pressure in the cavity of the part (evacuated by vacuum line) and the resin reservoir under ambient pressure. The filling ratio, the fiber volume fraction, is achieved by the equilibrium of forces between the resin reservoir and part compaction. For complete filling, the resin is spread by the resin line and a distribution media on the top surface of the component. Due to the part's large dimensions, tooling is one-sided, with an integrated heating system. The resulting challenge is achieving the temperature gradient between tooling and part surface, which becomes more significant with rising wall thicknesses and isolation materials. The resins used are mostly epoxy-based. To achieve an acceptable occupancy time for tooling, they are cured at temperatures of about 80 °C. During

this curing process, the epoxy resin's reaction is exothermic. This poses a process risk that the resin's limit temperature will be exceeded. Due to the laminate's low thermal conductivity, this risk increases with the thickness of laminates, which need to be reduced. Through the prediction of process temperatures, thermal damage to parts due to the melting of auxiliary materials, process-induced deformations [6] or laminate characteristics [7], can be avoided. Therefore, a simulation module for predicting the process temperatures in fiber-reinforced plastics with one-sided, heat able molds is required.

## 4.2 Application of Classical Laminate Theory

Classical Lamination Theory (CLT) is a commonly used predictive tool, which evolved in the 1960s, which makes it possible to analyze complex coupling effects that may occur in composite laminates. It is able to predict strains, displacements and curvatures that develop in a laminate as it is mechanically and thermally loaded. The method is similar to isotropic plate theory, with the main difference appearing in the lamina stress-strain relationships.



### 4.2.1 Hooke's law utilization in CLT

The Generalized Hooke's Law of stress and strain of any material is,

$$\begin{Bmatrix} \sigma_x \\ \sigma_y \\ \tau_{xy} \end{Bmatrix} = \begin{bmatrix} \overline{Q_{11}} & \overline{Q_{12}} & \overline{Q_{16}} \\ \overline{Q_{12}} & \overline{Q_{22}} & \overline{Q_{26}} \\ \overline{Q_{16}} & \overline{Q_{26}} & \overline{Q_{66}} \end{bmatrix} \begin{Bmatrix} \varepsilon_x \\ \varepsilon_y \\ \gamma_{xy} \end{Bmatrix}$$

$$\begin{Bmatrix} \sigma_x \\ \sigma_y \\ \tau_{xy} \end{Bmatrix} = \begin{bmatrix} \overline{Q_{11}} & \overline{Q_{12}} & 0 \\ \overline{Q_{12}} & \overline{Q_{22}} & 0 \\ 0 & 0 & \overline{Q_{66}} \end{bmatrix} \begin{Bmatrix} -\alpha_x \Delta T \\ -\alpha_y \Delta T \\ -\alpha_{xy} \Delta T \end{Bmatrix}$$

Where  $\overline{Q}$  is the stiffness matrix,  $\overline{Q}$  is the compliance matrix,  $\sigma$  are stress components,  $\varepsilon$  are strain components. The Generalized Hooke's Law for an Orthotropic Material reduces to;

A thin plate is a prismatic member having a small thickness, and it is the case for a typical lamina. If a plate is thin and there are no out-of-plane loads, it can be considered to be under plane stress. If the upper and lower surfaces of the plate are free from external loads, then,  $\sigma_z = \tau_{xz} = \tau_{yz} = 0$ . This assumption then reduces the three dimensional stress–strain equations to two-dimensional stress–strain equations.

A unidirectional lamina falls under the orthotropic material category. If the lamina is thin and does not carry any out-of-plane loads, one can assume plane stress conditions for the lamina. Therefore, taking, and, Equation (3.3) for an orthotropic plane stress problem can then be written as (3.4). Inverting Equation (3.4) stress–strain relationship is, (3.5). Where  $\overline{Q}$  are the reduced stiffness coefficients, which are related to the Compliance coefficients as  $\overline{Q} = [T]^{-1} [Q] [T]$ . Stiffness coefficients in terms of engineering or technical constants is

$$[T] = \begin{bmatrix} m^2 & n^2 & 2mn \\ n^2 & m^2 & -2mn \\ -mn & mn & m^2 - n^2 \end{bmatrix}; [Q] = [T]^{-1} \begin{bmatrix} \overline{Q_{11}} & \overline{Q_{12}} & \overline{Q_{16}} \\ \overline{Q_{12}} & \overline{Q_{22}} & \overline{Q_{26}} \\ \overline{Q_{16}} & \overline{Q_{26}} & \overline{Q_{66}} \end{bmatrix} [T]; \{\varepsilon\} = [T] \begin{Bmatrix} \varepsilon_x \\ \varepsilon_y \\ \gamma_{xy} \end{Bmatrix}$$

#### 4.2.2 Assumptions for Classical Laminate Theory

As with any analytical technique, some assumptions must be made in order to make the problem solvable:

1. The plate consists of orthotropic lamina bonded together, with the principal material axes of the orthotropic lamina orientated along arbitrary directions with respect to the x-y axes.
2. The thickness of the plate,  $t$ , is much smaller than any characteristic dimension.
3. The displacements  $u$ ,  $v$ , and  $w$  are small compared with  $t$ .
4. The in-plane strains  $\epsilon_x$ ,  $\epsilon_y$ , and  $\gamma_{xy}$  are small compared with unity.
5. Transverse shear is negligible,  $\gamma_{xz} = \gamma_{yz} = 0$  (plane stress in each ply).
6. Displacements  $u$  and  $v$  are assumed to be linear functions of the thickness coordinate  $z$  (no warping).
7. Assumptions 5 and 6 together define the Kirchhoff hypothesis.
8. Transverse normal strain  $\epsilon_z$  is negligible.
9. Each ply obeys Hooke's Law.
10. The plate thickness is constant throughout the laminate.
11. Transverse shear stress  $\tau_{xz}$  and  $\tau_{yz}$  vanish on the laminate surfaces  $z = \pm t/2$ .

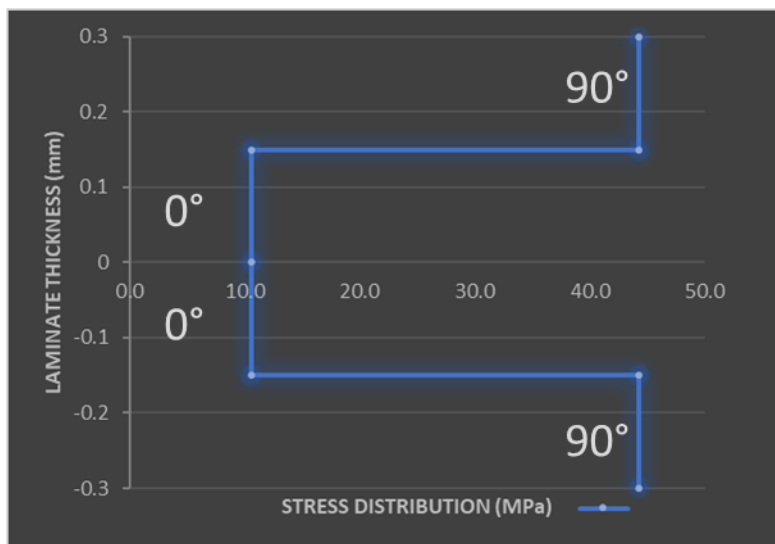
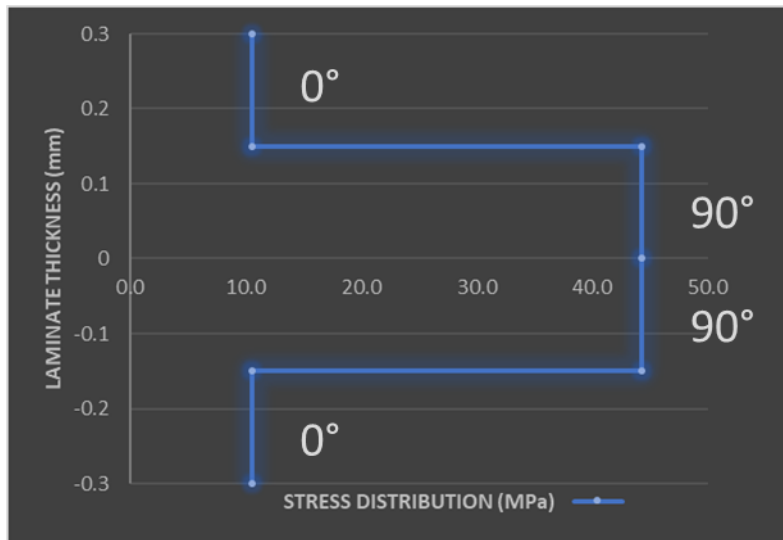
These assumptions lay the foundation for the theory and enable prediction of composite laminate behavior. More details will follow, so that we can understand the modifications made to the existing methodology.

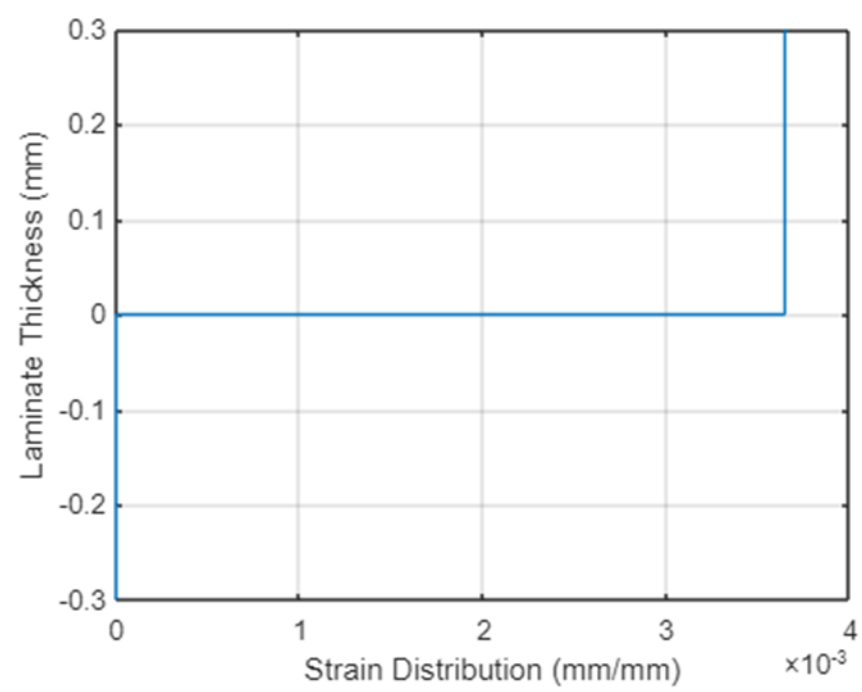
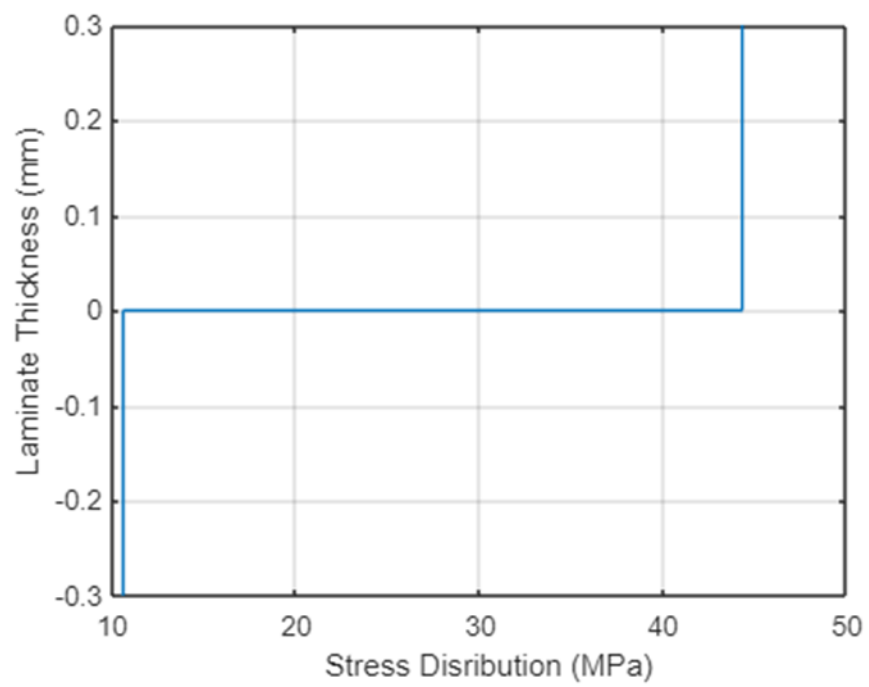
### ***4.2.3 Hooke's Law for Lamina under plane stress state***

A thin plate is a prismatic member having a small thickness, and it is the case for a typical lamina. If a plate is thin and there are no out-of-plane loads, it can be considered to be under plane stress. If the upper and lower surfaces of the plate are free from external loads, then, and. This assumption then reduces the three dimensional stress–strain equations to two-dimensional stress–strain equations.

A unidirectional lamina falls under the orthotropic material category. If the lamina is thin and does not carry any out-of-plane loads, one can assume plane stress Process Modelling with Thermosets.

#### 4.2.4 Stress Distribution in Symmetric and Non-Symmetric Laminate







#### 4.2.5 Resultant forces and moments due to thermal load

$$\begin{aligned}
 N_x^T &= \sum_{k=1}^N (Q_{11k} \alpha_{xk} + Q_{12k} \alpha_{yk} + Q_{16k} \alpha_{xyk})(z_k - z_{k-1}) \\
 N_y^T &= \sum_{k=1}^N (Q_{12k} \alpha_{xk} + Q_{22k} \alpha_{yk} + Q_{26k} \alpha_{xyk})(z_k - z_{k-1}) \\
 N_{xy}^T &= \sum_{k=1}^N (Q_{16k} \alpha_{xk} + Q_{26k} \alpha_{yk} + Q_{66k} \alpha_{xyk})(z_k - z_{k-1}) \\
 M_x^T &= \frac{1}{2} \sum_{k=1}^N (Q_{11k} \alpha_{xk} + Q_{12k} \alpha_{yk} + Q_{16k} \alpha_{xyk})(z_k^2 - z_{k-1}^2) \\
 M_y^T &= \frac{1}{2} \sum_{k=1}^N (Q_{12k} \alpha_{xk} + Q_{22k} \alpha_{yk} + Q_{26k} \alpha_{xyk})(z_k^2 - z_{k-1}^2) \\
 M_{xy}^T &= \frac{1}{2} \sum_{k=1}^N (Q_{16k} \alpha_{xk} + Q_{26k} \alpha_{yk} + Q_{66k} \alpha_{xyk})(z_k^2 - z_{k-1}^2)
 \end{aligned}$$

#### 4.2.6 Overall CTE for the laminate and total strain due to thermal load

$$\alpha_x = \frac{A_{22}N_x^T - A_{12}N_y^T}{A_{11}A_{22} - A_{12}^2} ; \alpha_y = \frac{A_{11}N_y^T - A_{12}N_x^T}{A_{11}A_{22} - A_{12}^2}$$

*Results,*

$$\alpha_x = -2.16 \times 10^{-6} / ^\circ C$$

&

$$\alpha_y = 16.80 \times 10^{-6} / ^\circ C$$

$$\varepsilon_x = 324 \times 10^{-6}$$

$$\varepsilon_y = -2520 \times 10^{-6}$$

#### 4.2.7 Residual stresses in the laminate due to thermal load

**RESIDUAL STRESSES:** (By applying Hook`s Law)

$$\{\sigma\} = \begin{Bmatrix} 53.4 \\ 14.64 \\ 0 \end{Bmatrix} \text{ MPa} \quad (\text{For } 0^\circ \text{ Layer})$$

$$\{\sigma\} = \begin{Bmatrix} -55.2 \\ 21.1 \\ -10.84 \end{Bmatrix} \text{ MPa} \quad (\text{For } 30^\circ \text{ Layer})$$

$$\{\sigma\} = \begin{Bmatrix} -55.2 \\ 21.1 \\ 10.84 \end{Bmatrix} \text{ MPa} \quad (\text{For } -30^\circ \text{ Layer})$$

#### 4.2.8 Thermal strain and change in height through the thickness

$$\varepsilon_{3k} = \alpha_{3k} \Delta T + S_{13k} \sigma_{1k} + S_{23k} \sigma_{2k}$$

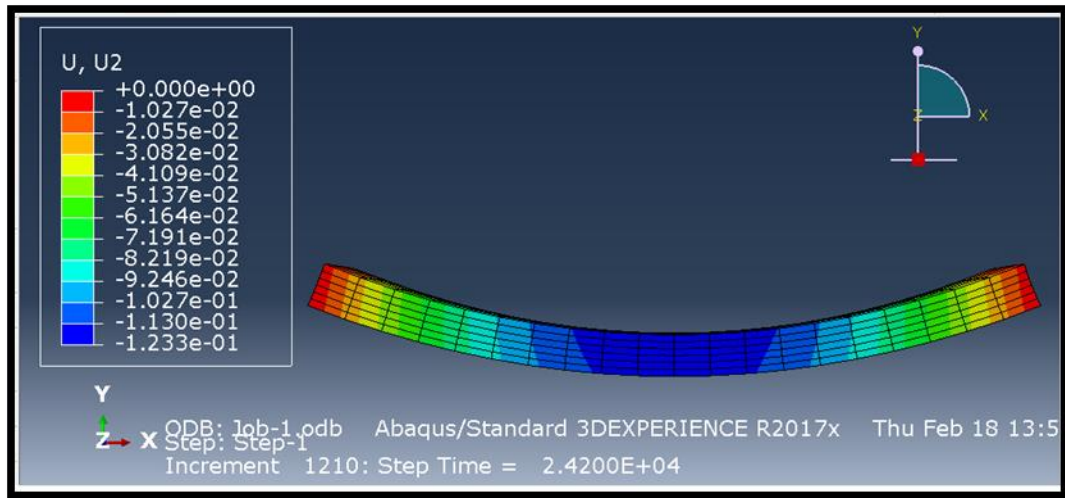
Where,

$$S_{13} = -\frac{\nu_{13}}{E_1} \quad \& \quad S_{23} = -\frac{\nu_{23}}{E_2}$$

$$\alpha_3 = 2.43 \times 10^{-5} / ^\circ C$$

$$\Delta h = \varepsilon_3 * h_o \quad \Rightarrow \quad h_k = h_o - \Delta h \quad \Rightarrow \quad \begin{Bmatrix} h_1 \\ h_2 \\ h_3 \\ h_4 \\ h_5 \\ h_6 \end{Bmatrix} = \begin{Bmatrix} 1.4934E - 04 \\ 2.9869E - 04 \\ 4.4804E - 04 \\ 5.9740E - 04 \\ 7.4675E - 04 \\ 8.9609E - 04 \end{Bmatrix} \text{ m}$$

#### 4.2.9 Validation of results through Abaqus Simulation



#### 4.2.10 Validation of results through CLT Software

LAMINATE PLY STRESSES, x-y COORDINATE SYSTEM:				
PLY NO	Z-COORD	SIGxx	SIGyy	TAUxy
1	-0.45000E+00	-0.26711E+02	-0.73218E+01	-0.38468E+02
	-0.30000E+00	-0.26711E+02	-0.73218E+01	-0.38468E+02
2	-0.30000E+00	-0.26711E+02	-0.73218E+01	0.38468E+02
	-0.15000E+00	-0.26711E+02	-0.73218E+01	0.38468E+02
3	-0.15000E+00	0.53423E+02	0.14644E+02	0.22026E-07
	0.29802E-07	0.53423E+02	0.14644E+02	-0.35981E-07
4	0.29802E-07	0.53423E+02	0.14644E+02	-0.35981E-07
	0.15000E+00	0.53423E+02	0.14644E+02	-0.93988E-07
5	0.15000E+00	-0.26711E+02	-0.73218E+01	0.38468E+02
	0.30000E+00	-0.26711E+02	-0.73218E+01	0.38468E+02
6	0.30000E+00	-0.26711E+02	-0.73218E+01	-0.38468E+02
	0.45000E+00	-0.26711E+02	-0.73218E+01	-0.38468E+02

$+30^\circ$

$-30^\circ$

$0^\circ$

$0^\circ$

$-30^\circ$

$+30^\circ$

### **4.3 Process Modelling with Thermosets**

### **4.4 Process Modelling with Thermoplastics**

# Chapter # 5

## **5 Results and discussion**

In this chapter, the results obtained from the pre-defined experimental matrix will be presented. These results include average velocity profiles, strain rate, shear, divergence from the velocity field, and swirling strength at different drilling parameters from PIV. Necessary figures and graphs will be presented, while complete sets of profiles can be viewed at the end.



# Chapter#6

## 6 Conclusion and recommendations

- Varying flow rate, drill pipe rotation and eccentricity, non-Newtonian fluid resulted considerable velocity change.
- Varying flow rate provides a higher velocity in the annulus, ultimately leads to an effective hole cleaning.
- Velocity profiles presented by the PIV gave information about the particle dynamics in annular flow and were used to describe the liquid-particle flow in a better way.
- At higher eccentricity of drill pipe (50%), Solid accumulated more at the bottom due to reduced annular area required to move the solid particles. The dune residence time increased, which was not desired phenomenon for horizontal drilling conditions.

### 6.1 Future Directions:

- The study was performed purely experimental. It would be interesting to compare the results with parametric CFD modelling.
- The characteristics of glass particles, i.e., particle size, shape, and overall concentration used in this thesis, were not changing. Literature indicates that changing characteristics affect cuttings transport. Changes in size, shape, and concentration would give a good indication of how large this effect will be.
- In the future, research papers will be published by applying these parameters in non-dimensional functions such as non-dimensional swirling coefficient, shear and shear rate, turbulence intensity, etc.

# Nomenclature

## Greek symbols

$\Delta \bar{x}$	Particle displacement
$\Delta t$	Amount of time
$\mu$	Fluid viscosity [kgm-1s-1]
$\lambda$	Ultrasonic wave length [ms-1Hz-1]
$\rho$	Fluid density [kgm-3]
$\tau$	Shear stress [Nm-2]

## Abbreviations

A	Area [m2]
$dv/dy$	Shear rate [s-1]
FFT	Fast Fourier Transform
ID	Inner diameter [mm]
LED	Light Emitting Diode
MB	Moving Bed
OD	Outer diameter [mm]
PIV	Particle Image Velocimetry
Re	Reynolds number



SB	Stationary Bed
----	----------------

# References

- Adrian, R J. 2005. "Twenty Years of Particle Image Velocimetry," 159–69. <https://doi.org/10.1007/s00348-005-0991-7>.
- Allahvirdizadeh, Payam, Ergun Kuru, and Mahmut Parlaktuna. 2016. "Experimental Investigation of Solids Transport in Horizontal Concentric Annuli Using Water and Drag Reducing Polymer-Based Fluids." *Journal of Natural Gas Science and Engineering* 35: 1070–78. <https://doi.org/10.1016/j.jngse.2016.09.052>.
- Ashwood, A. C., S. J. Vanden Hogen, M. A. Rodarte, C. R. Kopplin, D. J. Rodríguez, E. T. Hurlburt, and T. A. Shedd. 2015. "A Multiphase, Micro-Scale PIV Measurement Technique for Liquid Film Velocity Measurements in Annular Two-Phase Flow." *International Journal of Multiphase Flow* 68: 27–39. <https://doi.org/10.1016/j.ijmultiphaseflow.2014.09.003>.
- Balamurugan, R, and B Jeeva. 2019. "Micron Size Particle Image Velocimetry by Fast Fourier Transform Micron Size Particle Image Velocimetry by Fast Fourier Transform" 020156 (October).
- Bizhani, Majid, Ergun Kuru, and Sina Ghaemi. 2016. "Effect of near Wall Turbulence on the Particle Removal from Bed Deposits in Horizontal Wells." *Proceedings of the International Conference on Offshore Mechanics and Arctic Engineering - OMAE* 8: 1–10. <https://doi.org/10.1115/OMAE2016-54051>.
- Boiten, Maren Louise. 2016. "Experimental Study on Cuttings Transportation in Turbulent Pipe Flow." University of Stavanger.
- Brossard, C, J C Monnier, P Barricau, F X Vandernoot, Y Le Sant, G Le Besnerais, C Brossard, et al. 2015. "Principles and Applications of Particle Image Velocimetry." *Optical Diagnostics of Flows*, 19.
- Busahmin, Bashir, Nawaf H Saeid, Gamal Alusta, and El-said M M Zahran. 2017. "REVIEW ON HOLE CLEANING FOR HORIZONTAL WELLS" 12 (16): 4697–4708.
- CARLIER, JOHAN, and MICHEL STANISLAS. 2005. "Experimental Study of Eddy Structures in a Turbulent Boundary Layer Using Particle Image Velocimetry." *Journal of Fluid Mechanics*, 143–88. <https://doi.org/doi:10.1017/S0022112005004751>.
- CHAKRABORTY, PINAKI, S. BALACHANDAR, and RONALD J. ADRIAN. 2005. "On the Relationships between Local Vortex Identification Schemes." *Journal of Fluid Mechanics* 535: 189–

214. <https://doi.org/doi:10.1017/S0022112005004726>.
- Chang, Tae Hyun, and Kwon Soo Lee. 2010. "An Experimental Study on Swirling Flow in a Cylindrical Annuli Using the PIV Technique." *Journal of Visualization* 13 (4): 293–301. <https://doi.org/10.1007/s12650-010-0042-1>.
- Charogiannis, Alexandros, Jae Sik An, and Christos N. Markides. 2015. "A Simultaneous Planar Laser-Induced Fluorescence, Particle Image Velocimetry and Particle Tracking Velocimetry Technique for the Investigation of Thin Liquid-Film Flows." *Experimental Thermal and Fluid Science* 68: 516–36. <https://doi.org/10.1016/j.expthermflusci.2015.06.008>.
- Corredor, Fabio Ernesto Rodriguez, Majid Bizhani, and Ergun Kuru. 2013. "An Experimental Investigation of Turbulent Drag Reduction in Concentric Annulus Using Particle Image Velocimetry Technique." *Proceedings of the International Conference on Offshore Mechanics and Arctic Engineering - OMAE* 7: 1–17. <https://doi.org/10.1115/OMAE2013-11408>.
- GAO, Q., C. ORTIZ-DUEÑAS, and E. K. LONGMIRE. 2011. "Analysis of Vortex Populations in Turbulent Wall-Bounded Flows." *Journal of Fluid Mechanics* 678: 87–123. <https://doi.org/doi:10.1017/jfm.2011.101>.
- Girmaa, and Belayneh. 2013. "Cutting Transport Models and Parametric Studies in Vertical and Deviated Wells." University of Stavanger.
- Goharzadeh, A, and P Rodgers. 2009. "Experimental Characterization of Solid Particle Transport by Slug Flow Using Particle Image Velocimetry." *Journal of Physics: Conference Series* 147: 012069. <https://doi.org/10.1088/1742-6596/147/1/012069>.
- Imaging, Focus O NPhantom v7.3, v9.1, V10. n.d. "Product - Manual."
- Jahanmiri, Mohsen. 2011. "Particle Image Velocimetry : Fundamentals and Its Applications Particle Image Velocimetry : Fundamentals and Its Applications."
- Kopplin, Charles R. 2003. "LOCAL LIQUID VELOCITIES IN HORIZONTAL, ANNULAR AIR/WATER FLOW." In *Ring Congress & Exposition Proceedings of IMECE'03 2003 ASME International Mechanical Engineering Congress*, 1–5.
- "LaVision." n.d. <https://www.lavision.de/en/applications/fluid-mechanics/piv-system-components/>.
- LaVision GmbH. n.d. "No Title." <https://www.lavision.de/en/applications/fluid-mechanics/piv-system-components/seeding-particles/>.

- Lindken, Ralph, Massimiliano Rossi, Sebastian Große, and Jerry Westerweel. 2009. "Micro-Particle Image Velocimetry ( m PIV ): Recent Developments , Applications , and Guidelines †," 2551–67. <https://doi.org/10.1039/b906558j>.
- Manual, Product. n.d. "Sheet Optics ( Divergent ) LaVision."
- Messio, Laura, Cyprien Morize, Marc Rabaud, and Frédéric Moisy. 2008. "Experimental Observation Using Particle Image Velocimetry of Inertial Waves in a Rotating Fluid." *Experiments in Fluids* 44 (4): 519–28. <https://doi.org/10.1007/s00348-007-0410-3>.
- Nazari, T, G Hareland, and J J Azar. 2010. "SPE 132372 Review of Cuttings Transport in Directional Well Drilling : Systematic Approach."
- Raffel, Markus, Christian E Willert, Steve T Wereley, and Jürgen Kompenhans. 2007. *Particle Image Velocimetry - A Practical Guide*. Second. Springer.
- RATKOVSKÁ, Katarína. 2014. "Particle Image Velocimetry." Bohemia, Czeck Republic.
- Rodriguez-Corredor, F. E., Majid Bizhani, Mohammad Ashrafuzzaman, and Ergun Kuru. 2014. "An Experimental Investigation of Turbulent Water Flow in Concentric Annulus Using Particle Image Velocimetry Technique." *Journal of Fluids Engineering, Transactions of the ASME* 136 (5): 1–11. <https://doi.org/10.1115/1.4026136>.
- Rodriguez Corredor, Fabio E., Majid Bizhani, and Ergun Kuru. 2015. "Experimental Investigation of Drag Reducing Fluid Flow in Annular Geometry Using Particle Image Velocimetry Technique." *Journal of Fluids Engineering, Transactions of the ASME* 137 (8): 1–16. <https://doi.org/10.1115/1.4030287>.
- Santiago, J. G., S. T. Wereley, C. D. Meinhart, D. J. Beebe, and R. J. Adrian. 1998. "A Particle Image Velocimetry System for Microfluidics." *Experiments in Fluids* 25 (4): 316–19. <https://doi.org/10.1007/s003480050235>.
- Shi, Baocheng, Jinjia Wei, and Mingjun Pang. 2015. "A Modified Cross-Correlation Algorithm for PIV Image Processing of Particle-Fluid Two-Phase Flow." *Flow Measurement and Instrumentation*. <https://doi.org/10.1016/j.flowmeasinst.2015.06.010>.
- Sims, Karl. n.d. "No Title." <https://www.karlsims.com/fluid-flow.html>.
- Taso, Chih-Hsiang. 2018. "Assembling and Testing of PIV System Master Thesis." Technical University of Liberec.
- Webpage. n.d. "No Title." <https://www.web->

[formulas.com/Math\\_Formulas/Linear\\_Algebra\\_Divergence\\_of\\_a\\_Vector\\_Field.aspx](http://formulas.com/Math_Formulas/Linear_Algebra_Divergence_of_a_Vector_Field.aspx).

Wu, Qiong, Qian Ye, and Guoxiang Meng. 2013. "Particle Image Velocimetry Studies on the Swirling Flow Structure in the Vortex Gripper." *Proceedings of the Institution of Mechanical Engineers, Part C: Journal of Mechanical Engineering Science* 227 (9): 1927–37. <https://doi.org/10.1177/0954406212469323>.

## 7 List of tables

**Table 1 Physical and Chemical Properties of Flowzan.**-----Error! Bookmark not defined.

**Table 4 other available seeding particles (Raffel et al. 2007)**-----Error! Bookmark not defined.

## 8 List of figures

**Figure 1PIV setup on Multiphase flow loop in TAMUQ 259I Lab** Error! Bookmark not defined.

**Figure 45 With solid and drill pipe rotation of 120 RPM** Error! Bookmark not defined.